ACS OMEGA

http://pubs.acs.org/journal/acsodf

Article

One-Pot Synthesis of Polyoxometalate Decorated Polyindole for Energy Storage Supercapacitors

Anjana Anandan Vannathan, Tatinaidu Kella, Debaprasad Shee, and Sib Sankar Mal*

Cite This: *ACS Omega* 2021, 6, 11199−11208

Read Online

ACCESS | Metrics & More | Article Recommendations | Supporting Information

ABSTRACT: The demand for energy storage supercapacitor devices has increased interest in completing all innovative technologies and renewable energy requirements. Here, we report a simple method of two polyoxomolybdate ($H_4[PVMo_{11}O_{40}]$ and $H_5[PV_2Mo_{10}O_{40}]$) doped polyindole (PIn) composites for electrochemical supercapacitors. The interactions between polyoxomolybdates and PIn were measured by Fourier transform infrared spectroscopy (FTIR), and powder XRD, and stability was measured by thermogravimetry. The field emission scanning microscopy (FESEM) was employed to investigate the morphology of the materials. The electrochemical measurements show that the PIn/PV_2Mo_{10} electrode exhibits a higher capacitance of 198.09 F/g with an energy density of 10.19 Wh/kg and a power density of 198.54 W/kg at 0.2 A/g current density than the PIn/$PVMo_{11}$ electrode. Both electrodes show a pseudocapacitance behavior due to the doping of redox-active polyoxomolybdates on the PIn surface and enhance the electrochemical properties. The electrodes' capacitive nature was measured by electrochemical impedance spectroscopy (EIS), which shows that the PIn/$PVMo_{11}$ electrode has a resistive nature within the electrode−electrode interface. Moreover, the PIn/PV_2Mo_{10} electrode offers remarkable cycle stability, retaining ∼84% of its capacitance after 10,000 cycles (∼83% for the PIn/$PVMo_{11}$ electrode). The higher specific capacitance, faster charge/discharge rates, and higher cycle stability make them promising electrodes in supercapacitors.

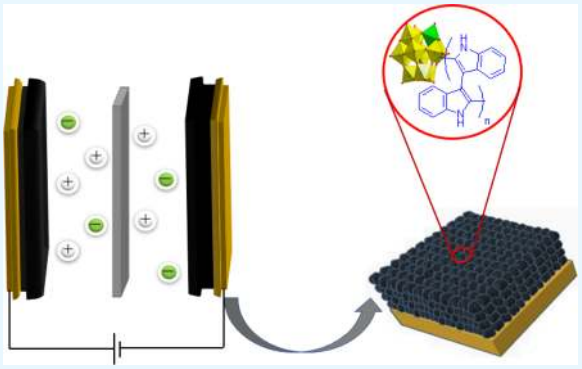

1. INTRODUCTION

The requirements of efficient energy storage devices have attracted tremendous interest in recent times due to the day-to-day utilization of portable electronic devices, mainly laptops, watch, mobile phones, etc. Moreover, the depletion of fossil fuels urge researchers to develop alternative green and sustainable energy storage systems.[1−3] On the other hand, sustainable and renewable energy is easily accessible and environment-friendly but cannot fulfill storage for the distant future because of its irregularities.[4,5] In this regard, electrochemical supercapacitors can store energy and deliver it even at higher rates than conventional batteries[6,7] because of their high power density, fast charge−discharge process, and long cycle life. However, less energy density placed the electrochemical capacitors below the Li-ion battery in the Ragone plot.[8] Nevertheless, the structural properties of the electrode materials define the performance of supercapacitors.[9−11]

To meet the demand for electronic storage devices, mainly carbonaceous-based supporting materials, such as graphene/metal oxides, graphene/conducting polymers, graphene/conducting polymers/metal oxides,[12,13] activated carbon (AC)/metal oxide,[14,15] carbon nanotube (CNT)/Co_3O_4,[16] graphdiyne,[17−19] SWCNT-polyoxometalate,[20] etc., were studied extensively. Recently, conducting organic polymers (COPs), mainly, polypyrrole (PPy), polyaniline (PAni), polythiophene (PTH), and poly(3,4-ethylene dioxythiophene) (PEDOT), attracted great interest in the field of energy storage device and were mostly explored due to the redox properties despite the swelling (oxidation)/shrinking (reduction) limitations during the charging−discharging process.[21] Furthermore, another COP, named polyindole (PIn), has immensely gained much attention in electrical energy storage. However, PIn is the least studied among the COPs owing to its low conductivity, mechanical strain over a long cycle, and material degradation, which leads to a loss in capacity and degradation (structural irregularities in the chain) of the storage device.[21] Despite suffering all the above properties, it bears some multiple advantages, including good thermal stability, stable redox activity,[22] photoluminescent properties,[23] electrochromic ability,[23] and slow degradation compared with polypyrrole and polyaniline.[24] Interestingly, PIn is a fused structure of poly(*p*-phenylene) and polypyrrole. Hence, it bears the

Received: December 10, 2020
Accepted: April 7, 2021
Published: April 22, 2021

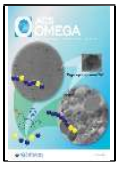

combination of both cyclic ring properties, which makes this material even more suitable for energy storage applications. The available literature on PIn in energy storage is scary due to its low conductivity.

The COPs were combined with the appropriate metal oxide to overcome all the challenges mentioned above, which would enhance the electrochemical performance because of the synergistic effect between them.[25] Among the various metal oxides investigated over the years; polyoxometalates are found attractive due to the unmatched range of physical and chemical properties, namely, redox properties (electrochemical performance), tuneable properties, thermal stability, etc.[26] Polyoxometalates are a class of multinuclear metal oxide nanoclusters that could be combined with conducting polymers (CPs). These composite materials were studied the most for the supercapacitor due to their "electron sponge" behaviors and enhanced electrochemical stability.[27] For example, White et al. prepared heteropolyacid-doped conducting polypyrrole, which was grown in the vapor phase, and a specific capacitance of about 422 F/g was reported.[28] Vaillant et al. synthesized the hybrid material PAni/PMo_{12} with the aid of H_2O_2, and the material showed a capacitance value of 168 F/g. The same group has prepared a new PEDOT/PMo_{12} hybrid electrode materials by a chemical method but obtained a low capacitance value of 130 F/g without H_2O_2.[29] Recently, Vannathan et al. synthesized two PPy/$H_4[PVMo_{11}O_{40}]$ and PPy/$H_5[PV_2Mo_{10}O_{40}]$ composites in situ, and a very high capacitance of 562 F/g was observed at 0.2 A/g in a H_2SO_4 electrolyte medium in two-electrode system.[30] Pedro Gomez-Romero et al. synthesized the PPy-Npipes, PW_{12}/PPy, and PMo_{12}/PPy and reported 204.5, 341, and 294.1 F/g of capacitance by using the three-electrode system in a 1 M H_2SO_4 electrolyte.[31] Cuentas-Gallegos et al. prepared $H_3PMo_{12}O_{40}$/PAni and found a 120 F/g specific capacitance in a two-electrode system, and they used Nafion117 and sulfuric acid as an electrolyte.[32] Jingjing Lin et al. synthesized Fe-Anderson-type polyoxometalate/polyaniline/graphene (PPG) and reported a 1366 F/g capacitance in the three-electrode system using 1 M H_2SO_4 as electrolyte.[33]

Surprisingly, there has not been any literature report on supercapacitors using doped polyoxometalates on polyindole-based conducting polymers to date due to the polymer material's low conductivity. We have decided to investigate the electrochemical studies of polyoxometalates doped on PIn and chose vanadium-based polyoxometalates for the oxidation–reduction nature of the vanadium.[20]

Herein, we report the first two new acidic Keggin polyoxomolybdates ($H_4[PVMo_{11}O_{40}]$, **$PVMo_{11}$**, and $H_5[PV_2Mo_{10}O_{40}]$, **PV_2Mo_{10}**) doped into the PIn matrix for the electrochemical performance and study the cycle stability of PIn-POMs in an aqueous acid electrolyte medium. Finally, all materials' supercapacitive properties were investigated by cyclic voltammetry (CV), galvanostatic charge/discharge (GCD), and electrochemical impedance spectroscopy (EIS) analysis. Hereafter, we refer to the two POMs using the abbreviations $PVMo_{11}$ and PV_2Mo_{10}, respectively.

2. RESULTS AND DISCUSSION

2.1. Physical Characterization of PIn, PIn/$PVMo_{11}$, and PIn/PV_2Mo_{10} Composites. Figure 1 depicts the comparative FTIR of polyindole (PIn), PIn/$PVMo_{11}$, and PIn/PV_2Mo_{10}. PIn revealed the characteristic absorption bands at 3400 (νN–H), 3000 (sp^2 C–H), 1619 and1490 (νC–C, Ar), 1460 (νC–N), 1365 (νC=N), and 741 cm^{-1} out-of-plane deformations (νC–H, Ar), respectively.[34] The FTIR of the two POMs ($PVMo_{11}$ and PV_2Mo_{10}) is reported elsewhere.[30] Figure 1B, C represents the FTIR of the PIn/$PVMo_{11}$ and PIn/PV_2Mo_{10} hybrid electrodes, which showed the retained chemical structure of both POMs ($PVMo_{11}$ and PV_2Mo_{10}) and characteristic bands at 1058 (1055, νP–O), 960 (961, νMo=O), and 744 (νV=O) cm^{-1}, respectively. Furthermore, the POM's characteristic bands were also observed in the hybrid materials and confirmed the impregnation of POMs on the PIn surface.

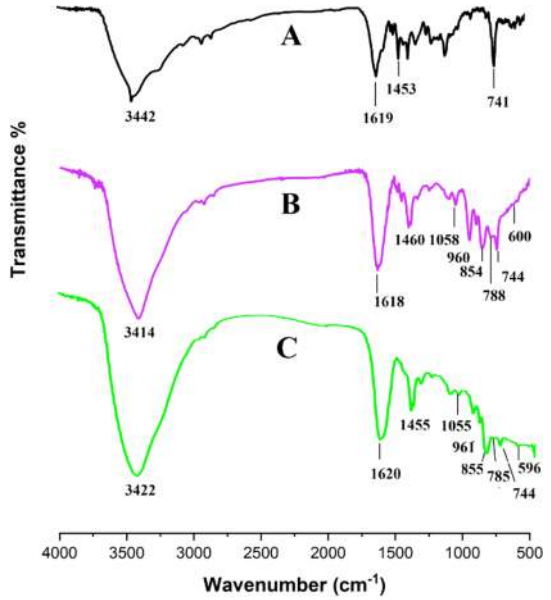

Figure 1. FTIR spectra of (A) PIn, (B) PIn/$PVMo_{11}$, and (C) PIn/PV_2Mo_{10}.

Figure 2 depicts the TGA of PIn, $PVMo_{11}$, PV_2Mo_{10}, PIn/$PVMo_{11}$, and PIn/PV_2Mo_{10} electrode materials. As seen from the thermal decomposition, doping of redox-active polyoxometalates increases the thermal stability of the electrodes. The DTG and the TGA curve of PIn (Figure S1a,b) show the first

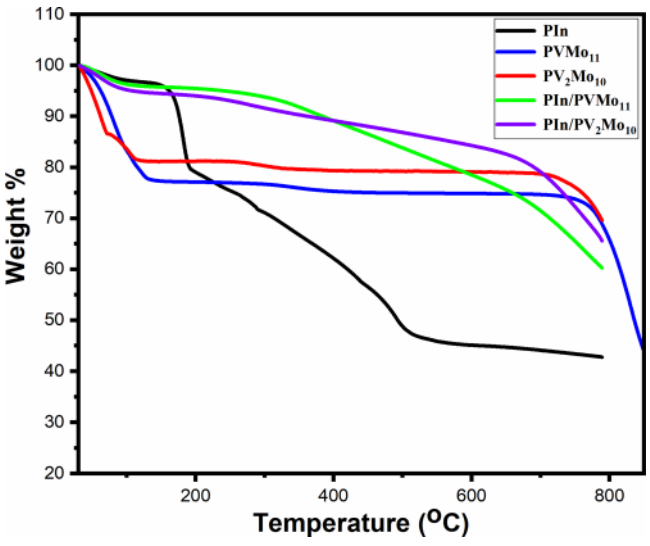

Figure 2. TGA of pure PIn, $PVMo_{11}$, PV_2Mo_{10}, PIn/$PVMo_{11}$, and PIn/PV_2Mo_{10}.

https://doi.org/10.1021/acsomega.0c05967
ACS Omega 2021, 6, 11199–11208

weight loss of 2.95% at 61.71 °C because of the moisture removal.[35] Several weight losses were observed after the glass transition temperature, which indicate the stagewise decomposition of the polymer backbone. The 50% weight loss of PIn was observed until 500 °C, which was prepared from the aqueous solution using $FeCl_3$ as an oxidant. The higher thermal stability of the PIn was varied, and it depends on the synthesis medium. For example, 50% weight loss was observed at 681.85 °C when synthesized from the CH_3CN/Bu_4NBF_4 medium.[36] In general, the PIn has a higher thermal stability, maybe due to the absence of counterions and a change in the molecular structure.[37,38] The weight loss of pure $PVMo_{11}$ and PV_2Mo_{10} (22.17 and 13.26%, Figure S1d,f) was observed until 123 and 101 °C for both POMs, ascribed to the expelling of the moisture and crystal water molecules, and further heating of both POMs exhibited utmost phase transition stability at 343.8 and 291.5 °C, respectively (Figure S1c,e). The thermal decomposition of both POMs is well documented in a published article.[30] The weight losses of doped $PVMo_{11}$ and PV_2Mo_{10} on PIn are depicted in Figure 2. The first weight loss of 3.55% at 63.56 °C corresponds to the moisture removal from the hybrid material (Figure S1g,h). The final weight loss (14.3%) until 765.81 °C is ascribed to the degradation of inorganic moieties of the $PIn/PVMo_{11}$. Likewise, the inorganic moieties in PIn/PV_2Mo_{10} decompose above 750 °C (Figure S1i,j). Figure 2 shows that both the $PIn/PVMo_{11}$ and PIn/PV_2Mo_{10} electrode materials are more stable than the pure PIn. In other words, the doping of POMs increased the stability of the electrode materials by many folds. This phenomenon can be explained by the synergistic interaction between the anionic $PVMo_{11}$ and PV_2Mo_{10} with PIn.

In agreement with the powder X-ray diffraction (P-XRD) patterns (Figure 3), the deposition of pure $PVMo_{11}$ and PV_2Mo_{10} on PIn shows the amorphous nature of $PIn/PVMo_{11}$ and PIn/PV_2Mo_{10} electrodes. The PIn shows characteristic broad peaks at 2θ = 7.89, 18.75, and 23.834° with 11.2, 4.73, and 3.73 Å lattice spacing and broad peaks indicating the microsphere structure of the material.[30] The P-XRD pattern of $PVMo_{11}$ showed peaks at 2θ of 9.7, 16.8, 21.8, 26.8, 27.6, 28.98, and 31.8° with a high percentage of crystalline material. Similarly, the P-XRD pattern of PV_2Mo_{10} showed similar diffraction angles (2θ) (9.76, 16.96, 21.41, 26.45, 27.75, 28.99, and 31.72°) and exhibited high crystalline material.[30] After doping both POMs on the backbone of PIn in situ, the number of diffraction angles was reduced, indicating the amorphous nature of the materials, and the loss of crystallinity of POMs is distinctly visible in Figure 3.

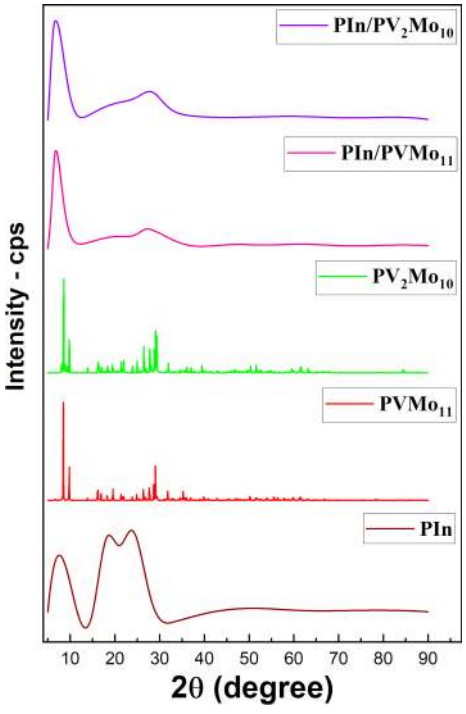

Figure 3. P-XRD pattern of PIn, $PVMo_{11}$, PV_2Mo_{10}, $PIn/PVMo_{11}$, and PIn/PV_2Mo_{10}.

To have further insight, the surface morphology (FESEM) of all the hybrid materials (PIn, $PIn/PVMo_{11}$, and PIn/PV_2Mo_{10}) was studied under identical conditions, which are presented in Figure 4A–C. FESEM reveals porous, rough surfaces with a nonuniform distribution of the PIn with 0.964 μm size (Figure 4A). Figure 4B, C shows the FESEM images of the two new $PIn/PVMo_{11}$ and PIn/PV_2Mo_{10} hybrid electrodes synthesized in situ by doping redox-active POMs on indole.

The morphologies of all materials reveal a characteristic nonuniform distribution rather than an accumulation of the composite's electrodes. Such morphology may arise due to the intercalation of the POMs in the PIn domain. Nevertheless, the morphology of PIn varies with the synthetic method and hence the capacitance. For example, Koiry et al. prepared long fiber-shaped PIn using $FeCl_3$ as an oxidant in an organic medium (dichloromethane) in a stationary interface. However, the PIn shape was changed to spherical when the interface was disturbed.[39] An et al. synthesized PIn by interfacial polymerization using $(NH_4)_2S_2O_8$ as an oxidizing agent in a chloroform medium. They observed a uniform nanoparticle formation with 1–3 mm diameter in size using cetyltrimethylammonium bromide as a surfactant.[40]

The energy dispersive X-ray (EDX) spectroscopy analysis was supported by the presence of all elements in PIn, $PIn/PVMo_{11}$, and PIn/PV_2Mo_{10}, as shown in Figure 4D–F. The EDX spectra confirmed C and N in pure PIn, and C, N, O, P, V, and Mo in the $PIn/PVMo_{11}$ and PIn/PV_2Mo_{10} hybrid electrodes, respectively. The FESEM and EDX of pure $PVMo_{11}$ and PV_2Mo_{10} are shown in Figure S2. The elemental compositions from EDX are presented in Table 1.

Figure 5 shows the N_2 adsorption/desorption isotherm of PIn, $PIn/PVMo_{11}$, and PIn/PV_2Mo_{10} materials. The specific BET surface area of PIn, $PIn/PVMo_{11}$, and PIn/PV_2Mo_{10} composites is 3.3, 7.52, and 9.3 m^2/g. The composite materials exhibited a type IV nitrogen adsorption isotherm without a defined hysteresis loop suggesting a nonporous nature, as shown in Figure 5. The lower surface area of newly synthesized electrode materials indicated a high amount of doping of $PVMo_{11}$ and $PV2Mo_{10}$ into the PIn surface and was fully integrated into the polymer matrix surfaces and may deliver substantial capacitance.

2.2. Electrochemical Characterization of the $PIn/PVMo_{11}$ and PIn/PV_2Mo_{10} Composites. The pseudocapacitive materials (e.g., transition metal oxide, conduction organic polymers) exhibit high specific capacitance and large energy density, making them ideal electrode materials for supercapacitors.[41−43] The electrochemical measurements of PIn, $PIn/PVMo_{11}$, and PIn/PV_2Mo_{10} electrodes were studied by cyclic voltammetry (CV) and galvanostatic charge–

https://doi.org/10.1021/acsomega.0c05967
ACS Omega 2021, 6, 11199−11208

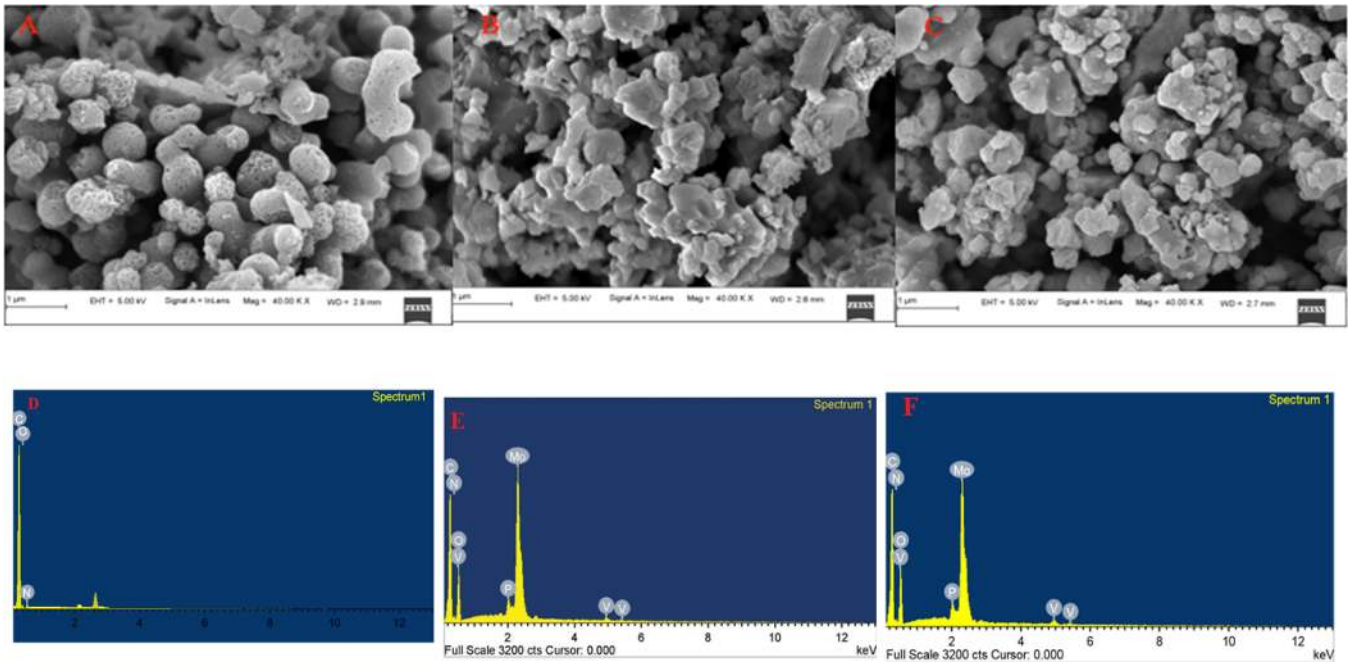

Figure 4. FESEM images of (A) pure PIn, (B) PIn/$PVMo_{11}$, and (C) PIn/PV_2Mo_{10}. EDX spectra of (D) pure PIn, (E) PIn/$PVMo_{11}$, and (F) PIn/PV_2Mo_{10}, respectively.

Table 1. Elemental Composition of PIn, PIn/$PVMo_{11}$, and PIn/PV_2Mo_{10} from EDX

	atomic (%)					
materials	N	O	C	P	V	Mo
PIn	23.73	50.84	25.42			
PIn/$PVMo_{11}$	1.79	53.83	28.71	1.02	1.11	13.54
PIn/PV_2Mo_{10}	6.06	52.62	26.31	1.20	1.05	12.76

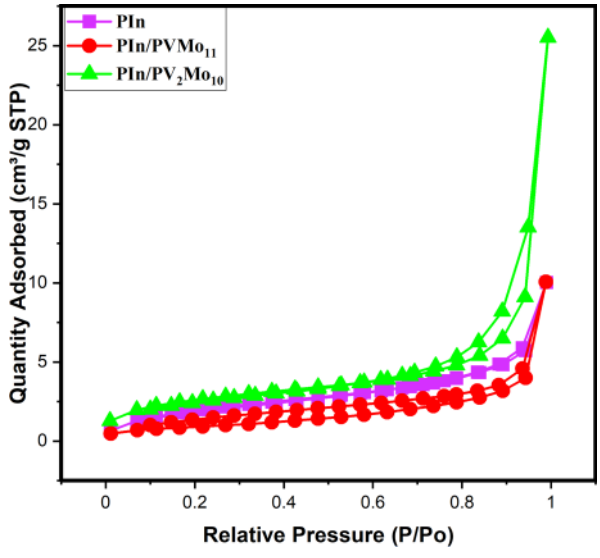

Figure 5. Nitrogen adsorption/desorption isotherm of PIn, PIn/$PVMo_{11}$, and PIn/PV_2Mo_{10} electrodes.

discharge (GCD) at 0.25 M H_2SO_4 electrolyte solution using two-electrode systems, as shown in Figure 6.

As depicted in Figure 6A, the pure PIn electrode's CV curves were determined at various scan rates from 5 to 100 mV/s. It reveals a quasi-rectangular shape without noticeable redox peaks, indicating an excellent electrical double-layer charge storage performance. The PIn has been considered a superior electrode material for supercapacitor due to the high thermal stability, slow degradation, and fast redox reaction.[44] However, the lower specific capacitance of pure PIn has been documented, which varies from the 93 to 114 F/g in various electrolyte solutions in three-electrode systems.[45,46] It exhibits low specific capacitance because of the low electrical conductivity compared to other CPs. Figure 6B shows a linear plot in the potential range of 0−1 V of charge−discharge curves, which exhibits a lower specific capacitance of 33.50 F/g at a lower current density (0.2 A/g).

Moreover, the PIn/$PVMo_{11}$ and PIn/PV_2Mo_{10} electrodes show the distorted rectangular shapes with a few redox peaks in the CV curves (Figure 6C, and E) with similar scan rates of 50−100 mV/s. This could be because of the pseudocapacitive behavior of both PIn and redox-active polyoxometalates ($PVMo_{11}$ and PV_2Mo_{10}). The specific capacitance was calculated to be 26.4 F/g for PIn/$PVMo_{11}$ and 60.81 F/g for PIn/PV_2Mo_{10} electrodes at the same scan rates of 5 mV/s (S1). The capacitance decreases with increasing scan rates for all the above cases due to the faster kinetics of ions at higher scan rates. Eventually, the electrolyte ion gets less time to penetrate the electrode.[38] The electrolyte ion's kinetic energy is reduced and has enough time to diffuse to the electrode surface, causing higher specific capacitance upon lowering the scan rates. The capacitance of PIn/$PVMo_{11}$ and PIn/PV_2Mo_{10} electrodes was estimated by GCD (Figure 6D, and F) measurements at various current densities. The pseudocapacitive nature of the electrodes could be visible in the charge−discharge curves, suggesting reversibility characteristics. The specific capacitance was estimated to be 177.36 and 198.54 F/g for PIn/$PVMo_{11}$ and PIn/PV_2Mo_{10} electrodes, respectively, at 0.2 A/g current density, significantly higher than the pure PIn under the same conditions (Table S1). The equation used for the calculations of specific capacitance, energy, and power density is given the Supporting Information (S1). The much

https://doi.org/10.1021/acsomega.0c05967
ACS Omega 2021, 6, 11199−11208

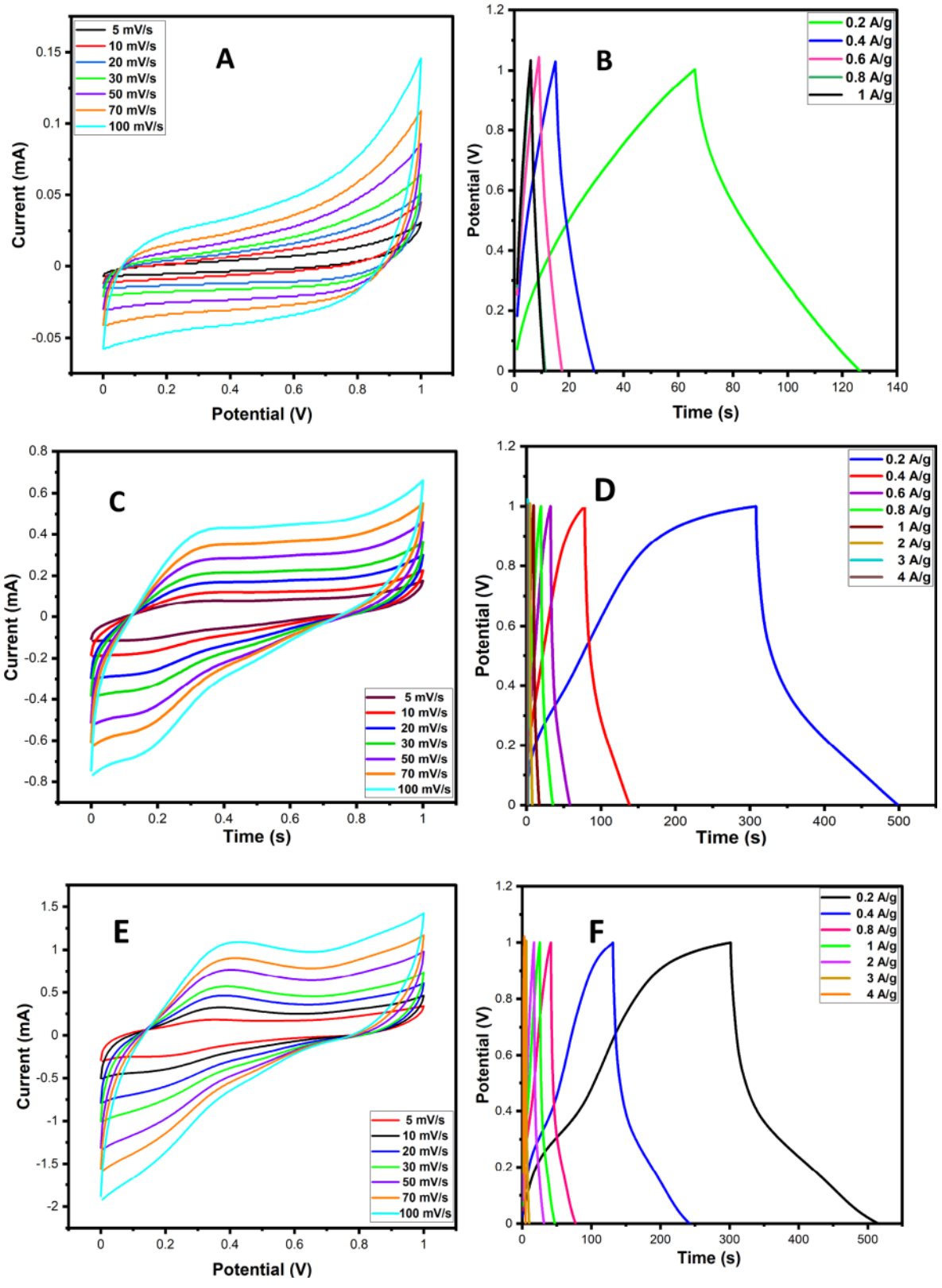

Figure 6. CVs of (A) PIn, (C) PIn/$PVMo_{11}$, and (E) PIn/PV_2Mo_{10} at various scan rates. GCD curves of (B) PIn, (D) PIn/$PVMo_{11}$, and (F) PIn/PV_2Mo_{10} with different current densities.

higher capacitance is probably due to the increment in the conductivity derived from the combination of redox-active polyoxometalates ions ($PVMo_{11}$ and PV_2Mo_{10}) with PIn. Simultaneously, the PIn/$PVMo_{11}$ and PIn/PV_2Mo_{10} electrodes displayed an energy density of 9.77 and 10.19 Wh/kg, respectively, at the same 0.2 A/g current density (Figure 7B, Table S1). As seen in Figure 6D, F, the specific capacitance values decrease with an increase in current density (Figure

https://doi.org/10.1021/acsomega.0c05967
ACS Omega 2021, 6, 11199−11208

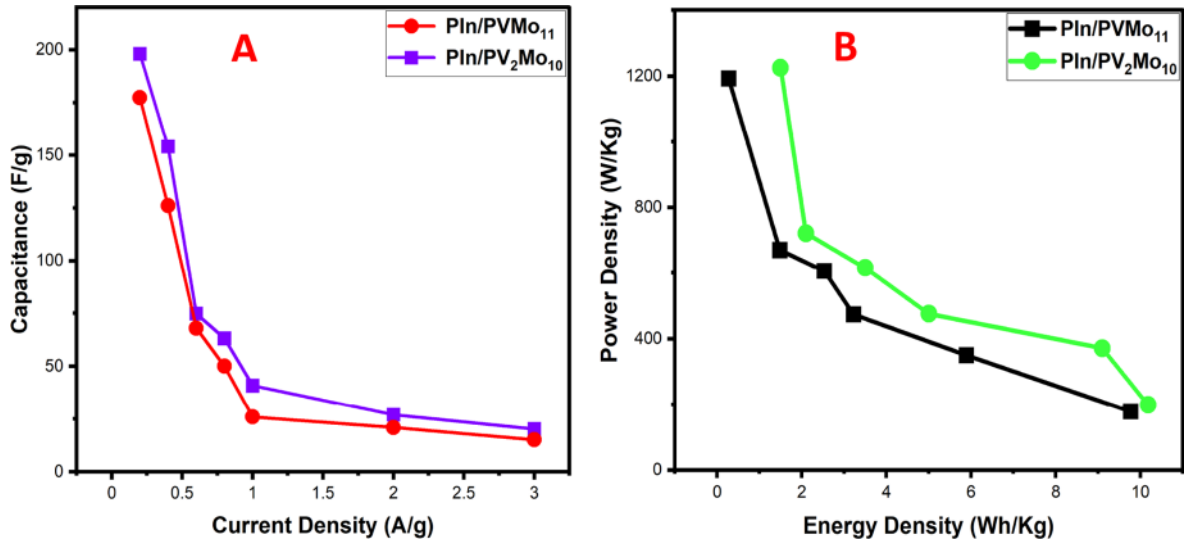

Figure 7. (A) Specific capacitance vs current density and (B) power density vs energy density of PIn/$PVMo_{11}$ and PIn/PV_2Mo_{10} electrodes.

7A), which illustrates that the electrochemical diffusion mechanism leads to energy storage. We envisaged the electrolyte ions' higher kinetic energy with less diffusion time with increasing current density.[47]

The electrochemical impedance spectroscopy (EIS) analysis has been performed to examine the resistance of both composite's electrode−electrode interface. All the data are presented as the Nyquist plot over 1 to 10^5 Hz frequency range (Figure 8) with 0.01 mV dc applied potential. In Figure 8, the insert pictured a small arc in the high-frequency region

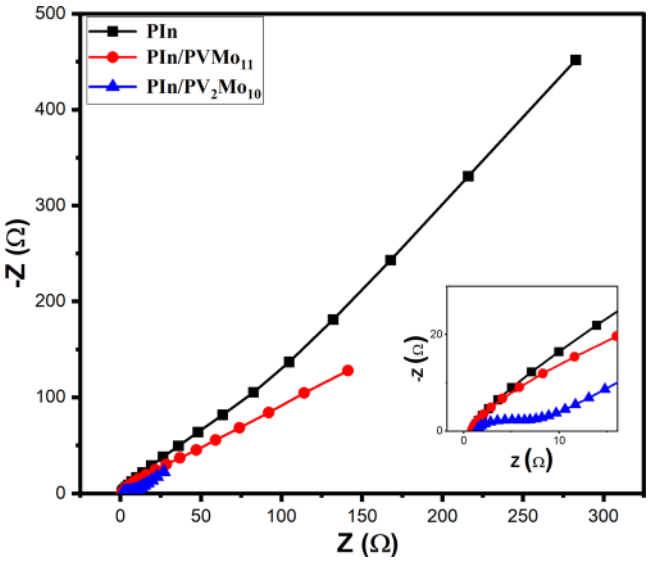

Figure 8. Nyquist plots for the PIn, PIn/$PVMo_{11}$, and PIn/ PV_2Mo_{10} electrodes.

for PIn/PV_2Mo_{10} electrodes, indicating the dominating supercapacitor's resistive nature within the electrode−electrode interface. Pure PIn and PIn/$PVMo_{11}$ have a minimal arc in the high frequency, suggesting the flawed resistive character.

The cell capacitance calculated based on the following eq 1 (*vide infra*) is shown in Table 2, and it was observed that the PIn/PV_2Mo_{10} electrode material could be applicable for a small cell.

$$C_{Tf} = 1/(2\pi f^{*}\mathrm{Im}[z]) \quad (1)$$

Table 2. Fitting Data of Equivalent Circuit Elements Obtained by Nyquist Plots

material	R_s (Ω)	R_{ct} (Ω)	R_p (Ω)	cell capacitance, $C_{Tf} = 1/2\pi f^{*}Im[z]$ *mF*	normalized to capacitance by using an active mass of the electrode (F/g)
PIn	0.98	4.03	5.01	0.56	1.4
PIn/ $PVMo_{11}$	0.88	4.93	5.82	1.13	2.825
PIn/ PV_2Mo_{10}	1.32	5.03	6.35	5.90	14.75

C_{Tf} is the cell capacitance, f is the minimum frequency applied, and $Im(z)$ is the complex impedance at the minimum frequency. So, the pseudocapacitance arises either from the electrolyte or redox reaction of PIn and POMs.[48−50]

The cell capacitance and impedance were estimated using the EIS data for the device (laboratory scale) applications, and details are available in the Supplementary Information (S1). The cell capacitance values of PIn, PIn/$PVMo_{11}$, and PIn/ PV_2Mo_{10} were calculated and observed to be 0.56, 1.13, and 5.9 mF, respectively (Table 2). The normalized capacitance by using an active mass of the electrode is 1.4, 2.8, and 14.75 F/g, respectively, for PIn, PIn/$PVMo_{11}$, and PIn/PV_2Mo_{10}.

The R_s, R_p, and R_{ct} were calculated from Figure 8, representing the electrolyte resistance in contact with the current collector/electrode and the electrode's internal resistance (R_p), and the charge transfer resistance of the redox reaction under course. As we know, the charge transfer resistance rises with the arch's diameter, eventually lowering the charge stored or discharged at the higher value of R_{ct}, indicating a higher pseudocapacitance. The PIn/PV_2Mo_{10} electrode shows a higher R_{ct} value of 5.03 Ω than other electrodes at room temperature (Table 2). It can be due to the presence of more vanadium atoms in the PV_2Mo_{10} Keggin polyanion, which helps to participate in the redox reaction.

https://doi.org/10.1021/acsomega.0c05967
ACS Omega 2021, 6, 11199−11208

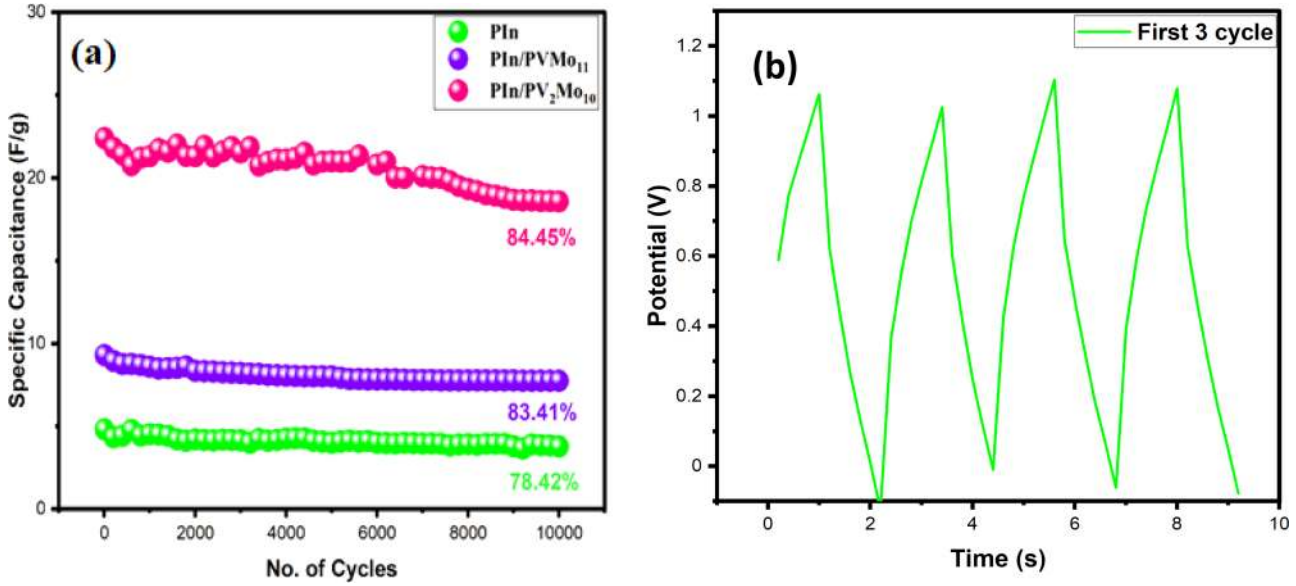

Figure 9. (a) Cycle stability of PIn, PIn/$PVMo_{11}$, and PIn/PV_2Mo_{10}. (b) The first three cycles of PIn/PV_2Mo_{10} are based on GCD.

An electrode's capacitance is hugely related to the mass and the device's size, considering the real-life application. For example, Pan et al. reported that for a small cell supercapacitor, the characteristic range of the cell capacitance is 1−10 mF (Table 1).[51] In this case, the PIn/PV_2Mo_{10} composite electrode shows the cell's capacitance value of ∼6 mF within the range of 1−10 mF and can be applied for small SC cell purposes.

2.3. Stability Performance of the Hybrid Electrodes. The capacitance retention plots of the PIn, PIn/$PVMo_{11}$, and PIn/PV_2Mo_{10}, respectively, shown in Figure 9a, which was measured based on the GCD curves at 4 A/g current density. After 10,000 cycles, the PIn, PIn/$PVMo_{11}$, and PIn/PV_2Mo_{10} electrodes retain their cycling stability of 78.4, 83.4, and 84.5%, respectively. The cycle stability of two pure POMs ($PVMo_{11}$ and PV_2Mo_{10}) has been reported elsewhere using the scan rate of 500 mV/s, and the $PVMo_{11}$ and PV_2Mo_{10} electrodes exhibit 68.7 and 71.3% retention stability, respectively, after 4500 cycles based on CV.[26] The PIn/PV_2Mo_{10} electrode offers the highest cyclic stability, and the first (Figure 9b) and last three cycles (Figure S3) of the PIn/PV_2Mo_{10} electrode show the electrode's excellent stability as compared to other electrodes materials. The first and last three cycles of other electrodes are represented in Figures S4 and S5.

3. CONCLUSIONS

In summary, we have synthesized two new PIn/$PVMo_{11}$ and PIn/PV_2Mo_{10} composite electrodes for the supercapacitor application. Furthermore, in the two-electrode cell configuration, the PIn/$PVMo_{11}$ and PIn/PV_2Mo_{10} nanostructure exhibits an upgraded specific capacitance value of 177.36 and 198.54 F/g, respectively in 0.25 M H_2SO_4 electrolyte. The PIn/PV_2Mo_{10} shows superior electrochemical faradic charge storage performance than PIn/$PVMo_{11}$, which might be attributed to the former's higher conductivity than the latter, and shows good reversibility of the electrode material. Again, the PIn/PV_2Mo_{10} electrode shows a high energy density of 10.19 Wh/kg and adequate cycle stability after 10,000 cycles at 4 A/g current density.

4. MATERIALS AND METHOD

Indole (99%) as a monomer was purchased from SRL Chem. Pvt. Ltd. NMP (*N*-methyl pyrrolidone) and carbon black were purchased from Sigma-Aldrich. Polyvinylidene (PDVF) was obtained from the Alfa Aesar. $NaVO_3$, Na_2MoO_4, Na_2HPO_4, HCl, H_2SO_4, and diethyl ether were purchased from Loba Chem. Pvt. Ltd. Carbon cloth was purchased from Sinergy Fuel Cell India Pvt. Ltd. Unless otherwise specified, all the reagents used were of analytical grade, and the solutions were made using HPLC-grade water. The redox-active polyoxometalate clusters $H_4[PVMo_{11}O_{40}]$ and $H_5[PV_2Mo_{10}O_{40}]$ were synthesized using the original synthesis method reported by Akba et al.[52]

Pure PIn was synthesized by a simple and inexpensive chemical method at room temperature. In this method, 1.0 g (0.04 mmol) of indole and 1.00 g (0.27 mmol) of $FeCl_3{\cdot}6H_2O$ were mixed in 50 mL of distilled water. The dark brown solid PIn started to form. The resulting solution was continuously stirred for 24 h at room temperature to complete the reaction. The dark brown solid was filtered off under vacuum using a membrane filter paper and washed several times with HPLC-grade water until the colorless filtrate's appearance. For polymerization reaction, monomers have to be oxidized to initiate the reaction. Here, $FeCl_3$ acts as an oxidizing agent and undergoes a free radical reaction for further polymerization. The synthesized composite's purity was checked by different analytical techniques, mainly FTIR, powder XRD, and finally EDX.[53]

4.1. Synthesis of PIn/$PVMo_{11}$ and PIn/PV_2Mo_{10} Composite Materials. *4.1.1. Synthesis of the PIn/$PVMo_{11}$ Composite.* The PIn/$PVMo_{11}$ was synthesized via an oxidative polymerization in situ method where $PVMo_{11}$ acts as an oxidant and Bronsted acid. One gram (0.12 mmol) of indole (monomer) was mixed with 50 mL of distilled water in a beaker. The indole/water mixture was stirred for a few minutes. Then, 2 g (4.75 mmol) of acidic $H_4[PVMo_{11}O_{40}]$ was added slowly to the indole/water mixture. The orange solution slowly turned to brown, and brown salt began to form. The resulting reaction was continuously stirred for 24 h at room temperature (Scheme 1). The deep brown solid was filtered off

https://doi.org/10.1021/acsomega.0c05967
ACS Omega 2021, 6, 11199−11208

Scheme 1. Schematic Representation of the Synthesis of the PIn/$PVMo_{11}$ and PIn/PV_2Mo_{10}

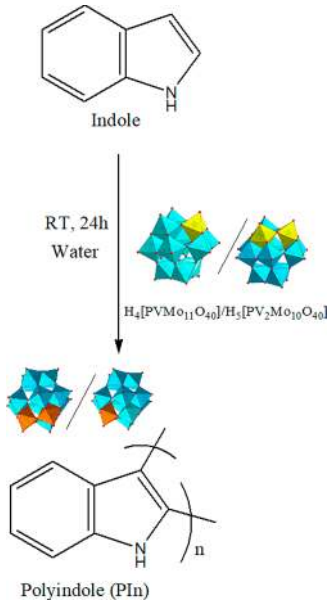

under vacuum by using a membrane filter paper and washed many times with HPLC-grade water until the filtrate appeared colorless to wash out excess POM present in the reaction medium. Finally, the substantial solid was air-dried, and we used it for our study. FTIR and powder XRD checked the purity of the synthesized composite. EDX measurements confirmed the elemental composition of all elements.

4.1.2. Synthesis of the PIn/PV_2Mo_{10} Composite. The PIn/PV_2Mo_{10} electrode was prepared similarly to PIn/$PVMo_{11}$, except that $H_5[PV_2Mo_{10}O_{40}]$ was used instead of $H_4[PVMo_{11}O_{40}]$ (Scheme 1).

4.2. Electrode Preparation. The electrode preparation is essential to determine the electrochemical properties of prepared materials. The electrodes were fabricated on a piece of carbon cloth (1 × 1, Synergic Pvt. Ltd.) by coating a slurry of active materials (PIn, PIn/$PVMo_{11}$, or PIn/PV_2Mo_{10}), carbon black, and polyvinylidene fluoride in the ratio of 80:10:10 with a few drops of *N*-methyl-2-pyrrolidone (NMP). The resulting slurry was sonicated for about $1^1/_2$ h, and the electrode materials (0.8 mg of the mass of the active material) were dispersed using a micropipette on the carbon cloth, followed by drying it over 24 h at 80 °C. The carbon cloth was rinsed with acetone and washed with HPLC grade water several times prior to use.

4.3. Instrumentation. The synthesized electrode materials were characterized by using different characterization techniques. FTIR spectra were acquired using a Bruker 4000 (USA) FTIR spectrometer in the wavenumber range of 4000−400 cm^{-1} to explore the material's chemical structure. The electrode material's thermal stability measurement was performed using a PerkinElmer TGA4000 (USA) using a heating rate of 5 °C/min inflowing of 20 mL/min N_2. The X-ray diffraction (XRD) patterns were acquired using a Rigaku Smartlab (Japan) diffractometer in the 2θ range of 10 to 90°. The field emission scanning electron microscopy (FESEM) (Carl Zeiss Sigma, Germany) image was acquired for all electrode materials to explore morphological properties. The specific BET surface area was determined in a Micromeritics physisorption analyzer (Model ASAP 2020, USA) using N_2 adsorption isotherm data collected at 77 K. The electrochemical performance of the prepared electrode material was performed using an electrochemical workstation (IVIUM Technologies BV Co., The Netherlands, Model: Vertex).

■ ASSOCIATED CONTENT

Supporting Information

The Supporting Information is available free of charge at https://pubs.acs.org/doi/10.1021/acsomega.0c05967.

TGA curves, FESEM and EDX, GCD of the last three cycles of PIn/PV_2Mo_{10}, GCD of the first and last three cycles of PIn/$PVMo_{10}$, GCD of the first and last three cycles of PIn, specific capacitance of composites, and calculations (PDF)

■ AUTHOR INFORMATION

Corresponding Author

Sib Sankar Mal − *Materials and Catalysis Laboratory, Department of Chemistry, National Institute of Technology Karnataka, Surathkal 575025, India;* orcid.org/0000-0002-2520-4371; Email: malss@nitk.edu.in

Authors

Anjana Anandan Vannathan − *Materials and Catalysis Laboratory, Department of Chemistry, National Institute of Technology Karnataka, Surathkal 575025, India*

Tatinaidu Kella − *Department of Chemical Engineering, Indian Institute of Technology Hyderabad, Sangareddy, Telangana 502285, India*

Debaprasad Shee − *Department of Chemical Engineering, Indian Institute of Technology Hyderabad, Sangareddy, Telangana 502285, India;* orcid.org/0000-0002-3503-8098

Complete contact information is available at: https://pubs.acs.org/10.1021/acsomega.0c05967

Notes

The authors declare no competing financial interest.

■ ACKNOWLEDGMENTS

This work is supported by the Council of Scientific and Industrial Research (CSIR) under scheme 01/(2906)/17/EMR-II, and A.A.V. thanks the National Institute of Technology Karnataka for financial assistance to carry out the research.

■ REFERENCES

(1) Xie, L.-J.; Wu, J.-F.; Chen, C.-M.; Zhang, C.-M.; Wan, L.; Wang, J.-L.; Kong, Q.-Q.; Lv, C.-X.; Li, K.-X.; Sun, G.-H. A Novel Asymmetric Supercapacitor with an Activated Carbon Cathode and a Reduced Graphene Oxide−Cobalt Oxide Nanocomposite Anode. *J. Power Sources* **2013**, *242*, 148−156.

(2) Xie, K.; Wei, B. Materials and Structures for Stretchable Energy Storage and Conversion Devices. *Adv. Mater.* **2014**, *26*, 3592−3617.

(3) Simon, P.; Gogotsi, Y. *Materials for Electrochemical Capacitors. In Nanoscience and Technology*; Co-Published with Macmillan Publishers Ltd: UK, 2009; pp. 320−329.

(4) Varun; Prakash, R.; Bhat, I. K. Life Cycle Greenhouse Gas Emissions Estimation for Small Hydropower Schemes in India. *Energy* **2012**, *44*, 498−508.

(5) Panwar, N. L.; Kaushik, S. C.; Kothari, S. Role of Renewable Energy Sources in Environmental Protection: A Review. *Renewable Sustainable Energy Rev.* **2011**, *15*, 1513−1524.

(6) Zhu, Y.; Murali, S.; Stoller, M. D.; Ganesh, K. J.; Cai, W.; Ferreira, P. J.; Pirkle, A.; Wallace, R. M.; Cychosz, K. A.; Thommes, M.; Su, D.; Stach, E. A.; Ruoff, R. S. Carbon-Based Supercapacitors Produced by Activation of Graphene. *Science* **2011**, *332*, 1537−1541.
(7) Miller, J. R.; Simon, P. MATERIALS SCIENCE: Electrochemical Capacitors for Energy Management. *Science* **2008**, *321*, 651−652.
(8) Cao, X.; Wang, X.; Cui, L.; Jiang, D.; Zheng, Y.; Liu, J. Strongly Coupled Nickel Boride/Graphene Hybrid as a Novel Electrode Material for Supercapacitors. *Chem. Eng. J.* **2017**, *327*, 1085−1092.
(9) Gueon, D.; Moon, J. H. MnO_2 Nanoflake-Shelled Carbon Nanotube Particles for High-Performance Supercapacitors. *ACS Sustainable Chem. Eng.* **2017**, *5*, 2445−2453.
(10) Yang, M.; Ko, S.; Im, J. S.; Choi, B. G. Free-Standing Molybdenum Disulfide/Graphene Composite Paper as a Binder- and Carbon-Free Anode for Lithium-Ion Batteries. *J. Power Sources* **2015**, *288*, 76−81.
(11) Zhang, X.-Q.; Sun, Q.; Dong, W.; Li, D.; Lu, A.-H.; Mu, J.-Q.; Li, W.-C. Synthesis of Superior Carbon Nanofibers with Large Aspect Ratio and Tunable Porosity for Electrochemical Energy Storage. *J. Mater. Chem. A* **2013**, *1*, 9449−9455.
(12) Stankovich, S.; Dikin, D. A.; Dommett, G. H. B.; Kohlhaas, K. M.; Zimney, E. J.; Stach, E. A.; Piner, R. D.; Nguyen, S. T.; Ruoff, R. S. Graphene-Based Composite Materials. *Nature* **2006**, *442*, 282−286.
(13) Shao, Y.; El-Kady, M. F.; Wang, L. J.; Zhang, Q.; Li, Y.; Wang, H.; Mousavi, M. F.; Kaner, R. B. Graphene-Based Materials for Flexible Supercapacitors. *Chem. Soc. Rev.* **2015**, *44*, 3639−3665.
(14) Suárez-Guevara, J.; Ruiz, V.; Gomez-Romero, P. Hybrid Energy Storage: High Voltage Aqueous Supercapacitors Based on Activated Carbon−Phosphotungstate Hybrid Materials. *J. Mater. Chem. A* **2014**, *2*, 1014−1021.
(15) Genovese, M.; Lian, K. Polyoxometalate Modified Pine Cone Biochar Carbon for Supercapacitor Electrodes. *J. Mater. Chem. A* **2017**, *5*, 3939−3947.
(16) Shan, Y.; Gao, L. Formation and Characterization of Multi-Walled Carbon Nanotubes/Co_3O_4 Nanocomposites for Supercapacitors. *Mater. Chem. Phys.* **2007**, *103*, 206−210.
(17) Shang, H.; Zuo, Z.; Zheng, H.; Li, K.; Tu, Z.; Yi, Y.; Liu, H.; Li, Y.; Li, Y. N-doped graphdiyne for high-performance electrochemical electrodes. *Nano Energy* **2018**, *44*, 144−154.
(18) Zuo, Z.; Li, Y. Emerging electrochemical energy application of graphdiyne. *Joule* **2019**, *3*, 899−903.
(19) Du, Y.; Zou, W.; Gao, J.; Pan, X.; Li, Y. Fundamental and application of graphdiyne in electrochemical energy. *Acc. Chem. Res.* **2020**, *53*, 459−469.
(20) Chen, H.-Y.; Al-Oweini, R.; Friedl, J.; Lee, C. Y.; Li, L.; Kortz, U.; Stimming, U.; Srinivasan, M. A Novel SWCNT-Polyoxometalate Nanohybrid Material as an Electrode for Electrochemical Supercapacitors. *Nanoscale* **2015**, *7*, 7934−7941.
(21) Gao, Y. Graphene and Polymer Composites for Supercapacitor Applications: A Review. *Nanoscale Res. Lett.* **2017**, *12*, 387.
(22) Xu, J.; Nie, G.; Zhang, S.; Han, X.; Hou, J.; Pu, S. Electrosyntheses of Freestanding Polyindole Films in Boron Trifluoride Diethyl Etherate. *J. Polym. Sci., Part A-1: Polym. Chem.* **2005**, *43*, 1444−1453.
(23) Trung, V. Q.; Huyen, D. N. Synthesis, Properties and Application of Polyindole/TiO_2 nanocomposites. *J. Phys.: Conf. Ser.* **2009**, *187*, No. 012058.
(24) Long, D.-L.; Tsunashima, R.; Cronin, L. Polyoxometalates: Building Blocks for Functional Nanoscale Systems. *Angew. Chem., Int. Ed.* **2010**, *49*, 1736−1758.
(25) Mai, L.-Q.; Minhas-Khan, A.; Tian, X.; Hercule, K. M.; Zhao, Y.-L.; Lin, X.; Xu, X. Synergistic Interaction between Redox-Active Electrolyte and Binder-Free Functionalized Carbon for Ultrahigh Supercapacitor Performance. *Nat. Commun.* **2013**, *4*, 2923.
(26) Gumerova, N. I.; Rompel, A. Synthesis, structures and applications of electron-rich polyoxometalates. *Nat. Rev. Chem.* **2018**, *2*, 0112.
(27) Kawasaki, N.; Wang, H.; Nakanishi, R.; Hamanaka, S.; Kitaura, R.; Shinohara, H.; Yokoyama, T.; Yoshikawa, H.; Awaga, K. Nanohybridization of Polyoxometalate Clusters and Single-Wall Carbon Nanotubes: Applications in Molecular Cluster Batteries. *Angew. Chem., Int. Ed.* **2011**, *123*, 3533−3536.
(28) White, A. M.; Slade, R. C. T. Investigation of Vapour-Grown Conductive Polymer/Heteropolyacid Electrodes. *Electrochim. Acta* **2003**, *48*, 2583−2588.
(29) Vaillant, J.; Lira-Cantu, M.; Cuentas-Gallegos, K.; Casañ-Pastor, N.; Gómez-Romero, P. Chemical Synthesis of Hybrid Materials Based on PAni and PEDOT with Polyoxometalates for Electrochemical Supercapacitors. *Prog. Solid State Chem.* **2006**, *34*, 147−159.
(30) Vannathan, A. A.; Maity, S.; Kella, T.; Shee, D.; Das, P. P.; Mal, S. S. In Situ Vanadophosphomolybdate Impregnated into Conducting Polypyrrole for Supercapacitor. *Electrochim. Acta* **2020**, *364*, 137286.
(31) Dubal, D. P.; Ballesteros, B.; Mohite, A. A.; Gómez-Romero, P. Functionalization of polypyrrole nanopipes with redox-active polyoxometalates for high energy density supercapacitors. *ChemSusChem* **2017**, *10*, 731−737.
(32) Cuentas-Gallegos, A. K.; Lira-Cantú, M.; Casañ-Pastor, N.; Gómez-Romero, P. Nanocomposite Hybrid Molecular Materials for Application in Solid-State Electrochemical Supercapacitors. *Adv. Funct. Mater.* **2005**, *15*, 1125−1133.
(33) Lin, J.; Yan, S.; Zhang, X.; Liu, Y.; Lian, J.; Lin, H.; Wei, W.; Lu, D.; Han, S. Facile preparation of holey Anderson-type polyoxometalate/polyaniline/graphene nanocomposites for supercapacitors. *NANO* **2019**, *14*, 1950049.
(34) Mudila, H.; Rana, S.; Zaidi, M. G. H.; Alam, S. Polyindole/Graphene Oxide Nanocomposites: The Novel Material for Electrochemical Energy Storage. *Fullerenes, Nanotubes, Carbon Nanostruct.* **2015**, *23*, 20−26.
(35) Anjitha, T.; Anilkumar, T.; Mathew, G.; Ramesan, M. T. Zinc ferrite @ polyindole nanocomposites: Synthesis, characterization and gas sensing applications. *Polym. Compos.* **2019**, *40*, 2802−2811.
(36) Choi, K. M.; Kim, C. Y.; Kim, K. H. Polymerization mechanism and physicochemical properties of electrochemically prepared polyindole tetrafluoroborate. *J. Phys. Chem.* **1992**, *96*, 3782−3788.
(37) Zhou, W.; Xu, J. Progress in Conjugated Polyindoles: Synthesis, Polymerization Mechanisms, Properties, and Applications. *Polym. Rev.* **2017**, *57*, 248−275.
(38) Zhou, Q.; Zhu, D.; Ma, X.; Xu, J.; Zhou, W.; Zhao, F. High-performance capacitive behavior of layered reduced graphene oxide and polyindole nanocomposite materials. *RSC Adv.* **2016**, *6*, 29840−29847.
(39) Koiry, S. P.; Saxena, V.; Sutar, D.; Bhattacharya, S.; Aswal, D. K.; Gupta, S. K.; Yakhmi, J. V. Interfacial Synthesis of Long Polyindole Fibers. *J. Appl. Polym. Sci.* **2007**, *103*, 595−599.
(40) An, S.; Abdiryim, T.; Ding, Y.; Nurulla, I. A Comparative Study of the Microemulsion and Interfacial Polymerization for Polyindole. *Mater. Lett.* **2008**, *62*, 935−938.
(41) He, S.; Cao, J.; Xie, S.; Deng, J.; Gao, Q.; Qiu, L.; Zhang, J.; Wang, L.; Hu, Y.; Peng, H. Stretchable Supercapacitor Based on a Cellular Structure. *J. Mater. Chem. A* **2016**, *4*, 10124−10129.
(42) Yang, P.; Mai, W. Flexible Solid-State Electrochemical Supercapacitors. *Nano Energy* **2014**, *8*, 274−290.
(43) Lu, X.; Yu, M.; Wang, G.; Tong, Y.; Li, Y. Flexible Solid-State Supercapacitors: Design, Fabrication and Applications. *Energy Environ. Sci.* **2014**, *7*, 2160−2181.
(44) Adhikari, A. D.; Oraon, R.; Tiwari, S. K.; Saren, P.; Lee, J. H.; Kim, N. H.; Nayak, G. C. CdS-$CoFe_2O_4$@Reduced Graphene Oxide Nanohybrid: An Excellent Electrode Material for Supercapacitor Applications. *Ind. Eng. Chem. Res.* **2018**, *57*, 1350−1360.
(45) Purty, B.; Choudhary, R. B.; Biswas, A.; Udayabhanu, G. Chemically grown mesoporous fCNT/α-MnO_2/PIn nanocomposites as electrode materials for supercapacitor application. *Polym. Bull.* **2019**, *76*, 1619−1640.
(46) Majumder, M.; Choudhary, R. B.; Koiry, S. P.; Thakur, A. K.; Kumar, U. Gravimetric and Volumetric Capacitive Performance of

https://doi.org/10.1021/acsomega.0c05967
ACS Omega 2021, 6, 11199−11208

Polyindole/Carbon Black/MoS2 Hybrid Electrode Material for Supercapacitor Applications. *Electrochim. Acta* **2017**, *248*, 98−111.
(47) Padmanathan, N.; Selladurai, S. Shape Controlled Synthesis of CeO_2 Nanostructures for High Performance Supercapacitor Electrodes. *RSC Adv.* **2014**, *4*, 6527−6534.
(48) lekha, P. C.; Subramanian, S.; Padiyan, D. P. Investigation of psudocapacitance effect and frequency dependence of ac impedance in polyaniline−polyoxometalate hybrids. *J. Mater. Sci.* **2009**, *44*, 6040−6053.
(49) Xiao, Q.; Zhou, X. The study of multi-walled carbon nanotube deposited with conducting polymer for supercapacitor. *Electrochim. Acta* **2003**, *48*, 575−580.
(50) Darowicki, K.; Kawula, J. Impedance characterization of the process of polyaniline first redox transformation after aniline electropolymerization. *Electrochim. Acta* **2004**, *49*, 4829−4839.
(51) Zhang, S.; Pan, N. Supercapacitors Performance Evaluation. *Adv. Energy Mater.* **2015**, *5*, 1401401.
(52) Akba, O.; Güzel, F.; Yurdakoc, K.; Gümgüm, B.; Tez, Z. Preparation and Characterization of Polyoxometallates of Molybdenum, Tungsten and Their Salts. *Synth. React. Inorg. Met.-Org. Chem.* **1997**, *27*, 1399−1415.
(53) Radhakrishnan, A.; Rejani, P.; Beena, B. CuO/Polypyrrole Nanocomposites as a Marker of Toxic Lead Ions for Ecological Remediation in Contrast with CuO and Polypyrrole. *Main Group Met. Chem.* **2015**, *38*, 133−143.

https://doi.org/10.1021/acsomega.0c05967
ACS Omega 2021, 6, 11199−11208